Acta Crystallographica Section D
Biological Crystallography
ISSN 1399-0047

Structural and bioinformatic characterization of an *Acinetobacter baumannii* type II carrier protein

C. Leigh Allen and Andrew M. Gulick*

Hauptman–Woodward Medical Research Institute and Department of Structural Biology, University at Buffalo, Buffalo, NY 14203, USA

Correspondence e-mail: gulick@hwi.buffalo.edu

Received 23 December 2013
Accepted 12 April 2014

PDB reference: NRPS PCP domain, 4hkg

Microorganisms produce a variety of natural products *via* secondary metabolic biosynthetic pathways. Two of these types of synthetic systems, the nonribosomal peptide synthetases (NRPSs) and polyketide synthases (PKSs), use large modular enzymes containing multiple catalytic domains in a single protein. These multidomain enzymes use an integrated carrier protein domain to transport the growing, covalently bound natural product to the neighboring catalytic domains for each step in the synthesis. Interestingly, some PKS and NRPS clusters contain free-standing domains that interact intermolecularly with other proteins. Being expressed outside the architecture of a multi-domain protein, these so-called type II proteins present challenges to understand the precise role they play. Additional structures of individual and multi-domain components of the NRPS enzymes will therefore provide a better understanding of the features that govern the domain interactions in these interesting enzyme systems. The high-resolution crystal structure of a free-standing carrier protein from *Acinetobacter baumannii* that belongs to a larger NRPS-containing operon, encoded by the ABBFA_003406–ABBFA_003399 genes of *A. baumannii* strain AB307-0294, that has been implicated in *A. baumannii* motility, quorum sensing and biofilm formation, is presented here. Comparison with the closest structural homologs of other carrier proteins identifies the requirements for a conserved glycine residue and additional important sequence and structural requirements within the regions that interact with partner proteins.

1. Introduction

Many microorganisms produce peptide natural products *via* novel secondary metabolic biosynthetic pathways (Gross & Loper, 2009; Li & Vederas, 2009; Meinwald, 2011). These products include the siderophore enterobactin, the biosurfactant surfactin, and antibiotics and cytostatic agents such as vancomycin and bleomycin, respectively, that have given rise to commercial therapeutics. These substances are all produced by nonribosomal peptide synthetases (NRPSs; Fischbach & Walsh, 2006). These molecular machines use a wide range of substrate amino acids to catalyze peptide synthesis independently of the ribosome.

The NRPSs use a modular catalytic strategy in which multiple protein activities that are required for the incorporation of a single amino acid into the final peptide define a single module. Typically, one module is present for each amino acid incorporated into the polypeptide. Most commonly, these multiple domains are joined in a single polypeptide, and large NRPSs that contain multiple modules and thousands of amino acids are not uncommon. During NRPS biosynthesis, the

© 2014 International Union of Crystallography

peptide intermediates are covalently attached to a peptidyl carrier protein (PCP) domain (Mercer & Burkart, 2007), which delivers the substrate to neighboring catalytic domains. The PCP domains are small ~75-residue units that are post-translationally modified with a phosphopantetheine cofactor that binds the amino acid and peptide intermediates as a thioester (Beld *et al.*, 2013). Unlike the more common multi-domain architecture, some NRPS systems contain catalytic and carrier domains expressed as single free-standing proteins. These so-called type II systems provide additional challenges that arise from the need for specific protein–protein interactions to govern proper biosynthesis.

A similar modular architecture is used by the polyketide synthase (PKS) machinery to incorporate malonate starter units into polyketide natural products. PKS enzymes also utilize integrated carrier proteins, described as ACPs to reflect the acyl substrates, that shuttle the polyketide intermediates between catalytic domains (Keatinge-Clay, 2012; Strieker *et al.*, 2010). Finally, fatty-acid synthase (FAS) enzymes use ACP domains to deliver the acyl groups to catalytic domains during the iterative elongation of fatty acids.

These three types of carrier proteins have been studied functionally, and structures of carrier domains have been determined by both crystallography and NMR. These structures illustrate that the carrier proteins adopt a common fold containing four helices (Crosby & Crump, 2012; Mercer & Burkart, 2007). Helices $\alpha1$, $\alpha2$ and $\alpha4$ are longer and are mostly parallel, while the shorter helix $\alpha3$ lies nearly perpendicular to the other three. The conserved serine residue that receives the phosphopantetheine cofactor lies at the start of helix $\alpha2$. The structural characterization of the holo and apo forms of the TycC3 PCP (Koglin *et al.*, 2006) illustrates multiple states of the protein in solution that are dynamically interconverting (designated the A and H states for the unique apo and holo states, respectively, as well as a third state that is shared by both apo and holo forms of the protein and is designated the A/H state). The authors of the recent crystal structure of BlmI (Lohman *et al.*, 2014), a type II PCP, note that carrier protein domains from X-ray crystal structures are predominantly in the A/H state and suggest that the alternate conformations observed for TycC3 may result from excising this carrier protein from the larger type I architecture.

Many human pathogens contain small NRPS clusters that are involved in the production of novel uncharacterized peptides. *Acinetobacter baumannii*, a Gram-negative bacterium that causes infectious outbreaks in multiple healthcare settings (Howard *et al.*, 2012), contains a small NRPS cluster derived from eight genes. Based on the presence of two adenylation domains (within a four-domain NPRS protein and the free-standing adenylation domain), this pathway is likely to form two separate acyl adenylates and is expected to produce a dipeptide or a derivative thereof.

This operon has been implicated in bacterial motility and quorum sensing (Clemmer *et al.*, 2011), two phenotypes that are dependent on the production of acyl-homoserine lactone signaling molecules. A random screen for mutants of the M-2 strain of *A. baumannii* that exhibit reduced motility identified transposon insertions into two genes within this operon (Clemmer *et al.*, 2011). These genes were additionally noted to be upregulated in response to quorum signals. Subsequently, transcriptome analysis of strain ATCC17978 demonstrated that mRNA encoding the type II carrier protein, annotated as gene A1S_0114, was exclusively expressed in biofilms and was not detected in planktonic cells (Rumbo-Feal *et al.*, 2013). Furthermore, the genes of this operon were overexpressed in biofilms by tenfold to 150-fold when compared with either exponential or stationary phase planktonic cell cultures. When the A1S_0114 gene was disrupted, there was an eightfold reduction in biofilm formation compared with the wild-type strain. Taken together, this evidence suggests that the carrier protein and this natural product operon are important in motility, quorum sensing and biofilm formation, phenotypes that are closely associated with bacterial virulence.

As an initial step towards understanding this uncharacterized NRPS pathway, we have subjected the core domains to structural investigation. Here, we report the structure of the free-standing carrier protein domain from this operon from *A. baumannii* strain AB307-0294 (Adams *et al.*, 2008). The biological function of this carrier protein is currently unknown; however, the co-translational expression of the operon suggests that this carrier domain may contribute a substrate to the NRPS system. Within the NRPS machinery, a type II PCP is a relatively rare occurrence. Du & Shen (1999) identified and characterized BlmI from the NRPS pathway involved in the synthesis of bleomycin, a protein that has recently been structurally characterized (Lohman *et al.*, 2014). Here, we present the crystal structure of this carrier protein and compare it with other carrier protein domains. Using features that have been described to distinguish the three types of carrier protein domains, we note that the *A. baumannii* carrier protein is more similar to the carrier proteins of natural product biosynthetic operons than to the ACPs of fatty-acid biosynthesis. We further characterize several conserved sequence motifs and compare the regions of the proteins that interact with biochemical partners.

2. Materials and methods

2.1. Cloning, expression and purification of A3404

For the overexpression of A3404[1] in *Escherichia coli*, we PCR-amplified the gene encoding A3404 (NCBI accession YP_002327276) from AB307-0294 genomic DNA and ligated the gene into the pET-15b-TEV expression vector (Kapust *et al.*, 2001). This yielded a construct that produced A3404 with a pentahistidine tag at the N-terminus that was cleaved by *Tobacco etch virus* (TEV) protease. The a3404 gene was cloned from *A. baumannii* strain AB307 genomic DNA (a gift from Dr Thomas Russo, University at Buffalo) by PCR. The

[1] The genes from strain AB307-0294 are annotated ABBFA_00####. For simplification, we will describe the genes as a####; the encoded proteins will be designated A####. Within the ATCC17978 and M-2 strains used in the genetic studies described in §1, the genes are annotated A1S_####. Both naming conventions are included in Fig. 1.

Table 1
Crystallographic and refinement data.

Values in parentheses are for the highest resolution shell. Because of the high noncrystallographic symmetry, the R_{free} reflections were generated in thin shells. The high-resolution R_{free} value is reported for data from 1.32 to 1.30 Å resolution.

Data collection	
Source	BL9-2, SSRL
Resolution (Å)	31.22–1.30
Space group	$P6_5$
Unit-cell parameters (Å, °)	$a = b = 61.81$, $c = 76.85$, $\alpha = \beta = 90$, $\gamma = 120$
R_{merge} (%)	6.0 (52.6)
Completeness (%)	99.1 (97.2)
$\langle I/\sigma(I)\rangle$	19.3 (5.7)
Multiplicity	10.3 (8.0)
Total reflections	415971
Unique reflections	40546
Refinement	
R_{cryst} (%)	14.9 (16.1)
R_{free} (%)	16.8 (16.6)
Wilson B factor (Å^2)	11.90
Average B factors (Å^2)	
Overall	16.7
Macromolecules	11.7
Solvent	27.0
R.m.s.d., bond lengths (Å)	0.005
R.m.s.d., angles (°)	1.00
No. of atoms	
Total	1624
Macromolecules	1294
Ligands	16
Water	311
Ramachandran favored (%)	98
Ramachandran outliers (%)	0
Clashscore†	2.24
PDB code	4hkg

† The *MolProbity* clashscore placed this structure in the 99th percentile.

primers used were 5′-ATT TTC AGG GC**C ATA TG**A ATA AAG ATA AAG CTT ACT GGA G-3′ and 5′-GTT AGC AGC C**GG ATC C**TC CTC ATG AAG CAA CTC CCT GC-3′. The 261-nucleotide gene was cloned using *Nde*I and *Bam*HI restriction sites (bold) into a modified pET-15b plasmid that contained a TEV protease site, and the sequence was confirmed by DNA sequencing. The resultant plasmid was used for expression in *E. coli* BL21(DE3) cells. Following inoculation with a small-scale overnight culture, a 1 l culture of cells was grown to an OD_{600} of ∼0.6 at 37°C and induced with 0.5 m*M* IPTG for 3 h. The cells were then pelleted by centrifugation and were either used immediately for protein purification or were flash-frozen in liquid nitrogen and stored at −80°C.

Cells were lysed by sonication in a buffer consisting of 50 m*M* HEPES (pH 7.5 at 4°C), 150 m*M* NaCl, 10 m*M* imidazole. The protein was purified by nickel ion-immobilized metal-affinity chromatography (IMAC). Following protein adsorption, the column was washed with 40 m*M* imidazole followed by elution of tagged A3404 with lysis buffer containing 300 m*M* imidazole. The purified protein was dialyzed overnight at 4°C against 1 l cleavage buffer consisting of 50 m*M* HEPES (pH 8.0 at 4°C), 150 m*M* NaCl, 0.5 m*M* EDTA with TEV protease included in the dialysis bag with the His_5-tagged protein and allowed to react overnight at 4°C during the dialysis step. The cleaved protein was passed over the same IMAC column and the untagged protein was collected in the flowthrough. The final protein, containing an N-terminal Gly-His sequence remaining after TEV cleavage, was dialyzed against 10 m*M* HEPES (pH 7.5 at 4°C), 50 m*M* NaCl. From 1 l of cells, ∼10 mg protein was obtained. The protein stock was frozen by pipetting directly into liquid nitrogen for storage at −80°C (Deng *et al.*, 2004).

2.2. Crystallization of A3404 and structure determination

Crystallization of apo A3404 was achieved *via* an initial screen with sparse-matrix conditions that utilized a broad array of PEG-based and salt-based precipitants (Carter & Carter, 1979; Jancarik & Kim, 1991). The final crystals of A3404 were grown at 4°C by hanging-drop vapor diffusion with a precipitant consisting of 25%(*v*/*v*) PEG 400, 5%(*v*/*v*) MPD, 0.2 m*M* TCEP, 50 m*M* CHES pH 9.0. Despite numerous attempts, we could not obtain crystals of the holo protein. Two sets of diffraction data were collected, with the first being collected at 100 K using a Rigaku MicroMax-007 microfocus X-ray generator, Osmic Max-Flux confocal focusing mirrors and a Saturn 944+ CCD detector. A higher resolution data set was subsequently collected using a wavelength of 0.9795 Å on SSRL beamline 9-2 equipped with a Si(111) double-crystal monochromator and a 325 mm MAR Mosaic CCD detector. Diffraction images were processed and scaled with the *HKL*-2000 suite (Otwinowski & Minor, 1997) and were converted to structure factors with *TRUNCATE* from the *CCP*4 software suite (Winn *et al.*, 2011).

The A3404 structure was initially determined by molecular replacement by using the first model (converted to poly-alanine) of the Asl1650 protein ensemble (Johnson *et al.*, 2006; PDB entry 2afd) as a search model against a data set collected on the home source. *EPMR* (Kissinger *et al.*, 2001) was used to identify the locations of the two molecules in the asymmetric unit. More than 20 models of ACP and PCP proteins were probed using multiple molecular-replacement programs before the successful search model was found using a poly-alanine chain derived from model 1 of PDB entry 2afd, an NMR structure with 29% identical (45% similar) residues to A3404. Following data collection to higher resolution, the low-resolution model was used with *Phaser* as utilized by the *PHENIX* (Adams *et al.*, 2010) molecular-replacement GUI. Refinement of the initial solution with *PHENIX* resulted in a model with an R_{cryst} of 14.9% (R_{free} of 16.8%).

The final model contains 1294 protein atoms and 311 solvent molecules. Additionally, there were two molecules of MPD bound near the pantetheine-binding motif in both subunits, a single molecule of ethylene glycol and a partial molecule of polyethylene glycol. Statistics for the data collection and refinement are presented in Table 1. The structure-based sequence alignment was generated with the *DALI* server (Holm & Rosenström, 2010); the structures were aligned with *CHIMERA* (Pettersen *et al.*, 2004).

3. Results and discussion

3.1. Sequence analysis of the *A. baumannii* NRPS cluster

The novel synthetic pathway encoded by *A. baumannii* under investigation in this work is approximately 15 kb of DNA in length and contains eight open reading frames (Fig. 1). This cluster has been identified in all available genomic sequences of *A. baumannii* (Adams *et al.*, 2008; Smith *et al.*, 2007; Vallenet *et al.*, 2008) and is not present in the nonpathogenic SDF strain or the related species *A. baylyi*. This predicted operon lies downstream of a transcriptional regulatory protein, ABBFA_003407, with homology to the PhzR and LuxR regulators as well as the acyl-homoserine lactone synthase CepI at ABBFA_003409.

The operon has all of the hallmarks of a pathway that produces a novel natural product. Gene a3399 encodes a phosphopantetheinyl transferase, or holo ACP synthase, that converts the carrier proteins from the apo to the holo state (Beld *et al.*, 2013). The operon encodes three NRPS proteins, an adenylation domain at a3406, a free-standing (type II) carrier protein at a3404 and a four-domain NRPS at a3403, which is composed of condensation, adenylation, carrier protein and thioesterase domains. A3404 is a free-standing carrier protein that could deliver a substrate to the NRPS system. Also encoded by the operon are two proteins, at a3400 and a3405, that show homology to NAD-dependent enzymes, as well as a hypothetical protein at a3401 that has no homology to characterized proteins but could function upstream or downstream to either generate alternate substrates or to modify the released product. Finally, the operon also encodes A3402, an efflux transporter that would be available to transport the final product outside of the cell.

The a3404 gene encodes a protein of 88 amino acids with a calculated pI of 4.22 and a molecular weight of 9643 Da. Similar to the carrier protein domains of NRPSs and the ACP domains of PKSs and FASs, A3404 has the highly conserved 4′-phosphopantetheinylation signature motif of GLDS. We examined this motif in the sequences of the more than 40 000 members of the Pfam family of carrier proteins, designated as PF00550, phosphopantetheine-attachment site. In this motif, the initial glycine three residues in front of the modified serine is observed in 91% of the family members. Two residues in front of the serine is a glycine (40%), leucine (19%), alanine (14%) or another hydrophobic residue such as valine or isoleucine (24% in total). The residue immediately in front of the serine is most commonly an aspartic acid (67%), histidine (17%) or asparagine (6%). This motif is thus best described as G-(G/L/A)-(D/H/N)-S.

3.2. Structure determination of A3404

The single-domain A3404 protein structure was initially determined using a data set collected on a home-source X-ray generator by molecular replacement with PDB entry 2afd as a

#	AB 307 orf	M2 orf	AAs	Proposed function
1	ABBFA_003406	A1S_0112	629	Adenylation (A) domain
2	ABBFA_003405	A1S_0113	597	Acyl-CoA dehydrogenase
3	ABBFA_003404	A1S_0114	86	Peptidyl carrier protein (PCP) domain
4	ABBFA_003403	A1S_0115	1319	Multi-domain NRPS protein containing condensation, A, PCP and thioesterase domains
5	ABBFA_003402	A1S_0116	1216	RND efflux transporter
6	ABBFA_003401	A1S_0117	423	Hypothetical
7	ABBFA_003400	A1S_0118	621	Homology to NAD-dependent epimerase/ dehydratase enzymes and esterases
8	ABBFA_003399	A1S_0119	256	4′-Phosphopantethienyl transferase

(*a*)

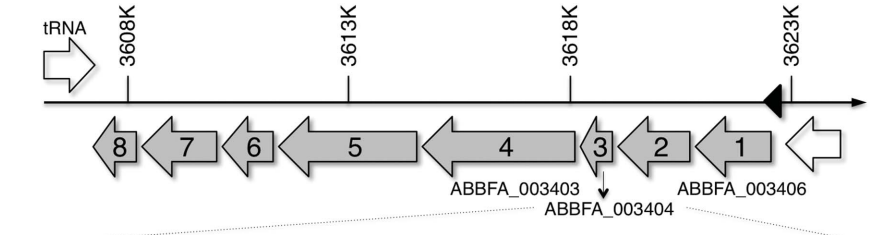


```
ATGAATAAAGATAAAGCTTACTGGAGCGCAATCATTCGTACGCTAGTCGCTAAAGAGATGCGCGTAGAGCCTGAGACG  78
M  N  K  D  K  A  Y  W  S  A  I  I  R  T  L  V  A  K  E  M  R  V  E  P  E  T
ATTGATCCAGATCAAAAATTTACCAGTTATGGTCTTGATTCGATTGTTGCTTTGTCTGTGTCTGGGGATTTAGAAGAT 156
I  D  P  D  Q  K  F  T  S  Y  G  L  D  S  I  V  A  L  S  V  S  G  D  L  E  D
CTGACGAAATTAGAACTTGAGCCGACACTATTATGGGATTACCCAACAATCAATGCGTTGGCCGAATATCTTGTTTCT 234
L  T  K  L  E  L  E  P  T  L  L  W  D  Y  P  T  I  N  A  L  A  E  Y  L  V  S
GAGCTGCAGCAGGGAGTTGCTTCATGA
E  L  Q  Q  G  V  A  S  *
```

(*b*)

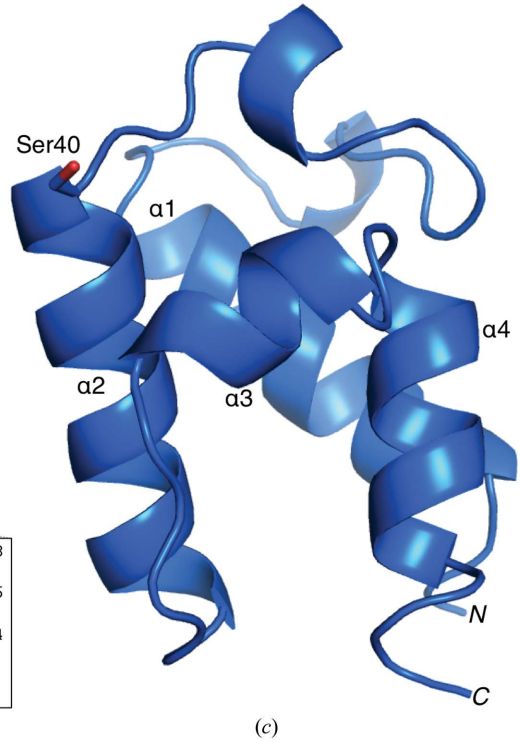

(*c*)

Figure 1
(*a*) The NRPS cluster from *A. baumannii* (with the gene nomenclature from both the AB307-0294 and ATCC17978/M2 strains). Protein sizes and proposed functions are included. (*b*) The genes are organized in a polycistronic operon containing eight genes (grey) preceded by a transcriptional regulatory protein (white). The sequences of the a3404 gene and protein are shown, with the carrier protein phosphopantetheinylation motif in red. (*c*) A ribbon diagram of A3404 highlights the four primary helices, α1–α4, and the long turn between the first two helices that contains two single-turn 3_{10}-helices. Ser40, the site of phosphopantetheinylation, is shown in a stick representation.

Table 2
Top unique homologs of A3404 from the *DALI* server (Z score > 10).

Molecule	PDB code	Type	Z†	R.m.s.d. (Å)	Res.‡	Align.§	Identity (%)	Method	Reference
CurA ACP_I	2liu	PKS ACP	14.0	1.0	99	80	30	NMR	Busche *et al.* (2011)
BlmI	4i4d	Type II NRPS PCP	13.9	1.6	83	78	19	X-ray	Lohman *et al.* (2014)
Protein ASL1650	2afd	PKS/NRPS carrier protein	13.0	1.4	88	79	32	NMR	Johnson *et al.* (2006)
Erythronolide synthase	2ju2	PKS ACP	12.0	1.6	95	79	29	NMR	Alekseyev *et al.* (2007)
EntF	3tej	NRPS PCP	11.5	2.0	320	72	19	X-ray	Liu *et al.* (2011)
TtACP	1x3o	*Thermus thermophilus* ACP	11.2	1.8	78	80	23	X-ray	RIKEN Structural Genomics/Proteomics Initiative (unpublished work)
Tyrocidine synthetase 3	2jgp	Type II NRPS PCP	11.0	1.9	520	74	19	X-ray	Samel *et al.* (2007)
SaACP	4dxe	*Staphylococcus aureus* ACP	10.7	1.8	75	77	16	X-ray	Center for Structural Genomics of Infectious Diseases (unpublished work)
Mupircin ACP	2l22	Tandem PKS ACP	10.6	1.8	76	183	22	NMR	Haines *et al.* (2013)
ScACP	2koq	*Streptomyces coelicolor* ACP	10.4	2.1	79	81	14	NMR	Płoskoń *et al.* (2010)
RcACP	2xz1	Rice ACP	10.4	2.2	76	82	18	X-ray	Guy *et al.* (2011)
PfACP	3gzm	*Plasmodium falciparum* ACP	10.2	2.0	77	81	18	X-ray	Gallagher & Prigge (2010)
RpACP	2kw2	*Rhodopseudomonas palustris* ACP	10.1	1.9	74	101	19	NMR	Ramelot *et al.* (2012)
SoACP	2fve	Spinach ACP	10.0	2.1	77	82	18	NMR	Zornetzer *et al.* (2006)

† The Z-score is a pairwise comparison score to allow ranking of the results. ‡ The number of total residues in a given structure. § The number of residues that were aligned with the query sequence (A3404).

search model. Following higher resolution data collection, the structure in progress was used as a model for molecular replacement. The asymmetric unit contains two A3404 monomers. The final model of A3404 contains 81 residues for each chain; both monomers are missing Gly−1 and His0, remnants from the N-terminal purification tag that remain after TEV cleavage, and Met1, as well as five C-terminal residues (Gln82–Ser86). Crystallographic and refinement data statistics are shown in Table 1.

The domain structure of A3404 is the archetypal carrier protein consisting of four α-helices. The conserved serine that is the site of the 4′-phosphopantetheinylation modification, Ser40, is positioned at the N-terminal end of the second helix (Fig. 1). Multiple carrier protein structures from NRPS clusters and ACPs from PKS and FAS systems have been determined by X-ray crystallography and NMR (Crosby & Crump, 2012; Mercer & Burkart, 2007). Although there is significant structural variation among the previous structures, nearly all structures retain the four main helices. An extended loop joins helices α1 and α2. In the case of A3404, this loop contains two single-turn 3_{10}-helices. While helices α1, α2 and α4 are of similar lengths and are roughly parallel, helix α3 is shorter and is nearly perpendicular to helices α2 and α4. Using the *DALI* alignment server (Holm & Rosenström, 2010), the 14 closest structural homologs to A3404 were determined (all resulting in Z-scores greater than 10; Table 2). Within these structures, the sequence similarity ranged from 13% for an inhibitor-bound adenylation-PCP domain module from *Pseudomonas aeruginosa* (Mitchell *et al.*, 2012) to 32% for the 2afd structure (Johnson *et al.*, 2006) that was used as a model for molecular replacement. This sampling of structures, which included a wide array of representative carrier proteins, all had less than 2.5 Å root-mean-square displacement of C^{α} positions. Interestingly, the list of the proteins that are the closest homologs contains equal numbers of structures determined by X-ray crystallography and by NMR spectroscopy.

3.3. Comparison of the structure of A3404 to other carrier proteins

The classification of carrier proteins into one of the three classes based on sequence or structure alone can be difficult and, indeed, genomic context is another important tool that should be considered. The co-expression of A3404 with the adenylation domain of A3406 and the four-domain NRPS protein at A3403 suggests that this protein will serve in a natural product pathway. We therefore examined the 14 protein structures that were most closely related as predicted by the *DALI* server more closely. Interestingly, the 14 proteins contain seven ACPs from fatty-acid synthesis and transport and seven proteins from natural product (NRPS or PKS) pathways. The top five proteins as scored by *DALI*, and six of the top seven, are all from natural product systems. One protein, a carrier protein from *Anabaena*, is of unclear function; however, the authors considered it to be a carrier protein for either an NRPS or PKS (or hybrid) cluster (Johnson *et al.*, 2006).

The regions of the carrier protein that are most important for distinguishing among the different types are the loop between helix α1 and α2, the α2 helix itself and the α3 helix (Crosby & Crump, 2012; Lai *et al.*, 2006; Lohman *et al.*, 2014; Mercer & Burkart, 2007). Not surprisingly, these are the regions of the proteins that interact with partner proteins, largely owing to the proximity to the site of loading at the start of the α2 helix. We examined the multiple sequence alignment generated from *DALI* and additionally examined the structures of each protein compared with A3404 (Fig. 2). This limited alignment of closely related structures provides some insight into the comparison between the three types of carrier protein. Firstly, we examined the sequence of the pantetheine-binding motif. Of interest, all ACPs, whether from FAS or PKS systems, contained an aspartic acid immediately preceding the serine residue. This trend is consistent with larger alignments presented by others (Crosby & Crump, 2012; Lohman *et al.*,

2014); however, exceptions are clearly present. The acidic nature of the hydrophilic face of helix $\alpha2$ is also quite striking. All FAS ACPs except for PDB entry 2koq contain acidic residues at the second and fifth residues following the pantetheinylated serine and are much more highly acidic at the C-terminal end of the helix. Similarly, the amino acids that immediately precede helix $\alpha3$ also are much more highly acidic in the FAS ACP sequences. These two features are also similar to the observations used to characterize the Asl1650 carrier protein (Johnson *et al.*, 2006).

The structure of A3404 was compared with all 14 of the most closely related ACP structures, and structural alignments for the two most similar structures of each class are shown in Fig. 2(*b*). The structure of the ACP from the curamicin PKS (PDB entry 2liu) illustrates the best alignment with A3404, which is also reflected by the lowest r.m.s. displacement of C^{α} positions (Table 2). In particular, the path traced by the main chain in the divergent loop between helices $\alpha1$ and $\alpha2$ and the $\alpha3$ helix are very similar. The positional conservation with a second PKS ACP is also quite good, although differences in the position of the second 3_{10}-helix of the loop that precedes helix $\alpha2$ are more pronounced. The comparison with the two NRPS PCP structures, BlmI and EntF, show comparable overall similarities. A noteworthy difference is the lack of the first 3_{10}-helix in the two PCP structures. Finally, comparison of the A3404 structure with the FAS ACP structures shows larger

```
        3404    NKDKAYWSAIIRTLVAKEMRVEPETIDPDQKFTSYGLDSIVALSVSGDLEDLTKLELEPTLLWDYPTINALAEYLVSELQ
 1 PKS  2liu    QVNLSEIKQVLKQQLAEALYTEESEIAEDQKFVDLGLDSIVGVEWTTTINQTYNLNLKATKLYDYPTLLELSGYIAQILS
 2 NRPS 4i4d    RTRRRALERDIAAIWAETLGRDS--VGPHEDFAALGGNSIHAIKITNRVEELVDAELSIRVLLETRTVAGMTDHVHATLT
 3 P/N  2afd    -ASVEDIQSWLIDQFAQQLDVDPDDIDMEESFDNYDLNSSKALILLGRLEKWLGKELNPVLIFNYPTIAQLAKRLGELYL
 4 PKS  2ju2    AERTAELVRLVRTSTATVLGHDPKAVRATTPFKELGFDSLAAVRLRNLLNAATGLRLPSTLVFDHPNASAVAGFLDAELG
 5 NRPS 3tej    ----AGSETIIAAAFSSLLGC----QDADADFFALGGHSLLAMKLAAQLSRQVARQVTPGQVMVASTVAKLATIIDAEED
 7 NRPS 2jgp    ----SVWEARLAQVWEQVLNVP--QVGALDDFFALGGHSLRAMRVLSSMHNEYQVDIPLRILFEKPTIQELAAFIEETAK
 9 PKS  2l22    ----DECAQFLRQSLAAMLYCEPGQIRDGSRFLELGLDSVIAAQWIREINKHYQLKIPADGIYTYPVFKAFTQWVGTQLQ

 6 ACP  1x3o    -MTEQEIFEKVKAVIADKLQVEPEKVTLEARFIEDGADSLDTVELIMGLEDEFGLEIS-EEAEKIRTVKDAVEYIKAKLG
 8 ACP  4dxe    --NAMENFDKVKDIIVDRLGVDADKVTEDASFKDLGADSLDIAELVMELEDEFGTEIP-EEAEKINTVGDAVKFINSL--
10 ACP  2koq    -ATQEEIVAGLAEIVNEIAGIPVEDVKLDKSFDDLDVDSLSMVEVVVAAEERFDVKIPDDDVKNLKTVGDATKYILDHQA
11 ACP  2xz1    --AKKETIDKVSDIVKEKLALG-VVVTADSEFSKLGADSLDTVEIVMNLEEEFGINVEDKA-QDISTIQQAADVIEGLLE
12 ACP  3gzm    --SLKSTFDDIKKIISKQLSVEEDKIQMNSNFTKDGADSLDLVELIMALEEKFNVTIDQDA-LKINTVQDAIDYIEKNN-
13 ACP  2kw2    ----TSTFDRVATIIAETCDIPRETITPESHAIDLGIDSLDFLDIAFAIDKAFGIKLPLE--EQYFVLKNLAARIDELVA
14 ACP  2fve    --AKKETIDKVSDIVKEKLALG-VVVTADSEFSKLGADSLDTVEIVMNLEEEFGINVEDEKAQDISTIQQAADVIEGLLE
```

(*a*)

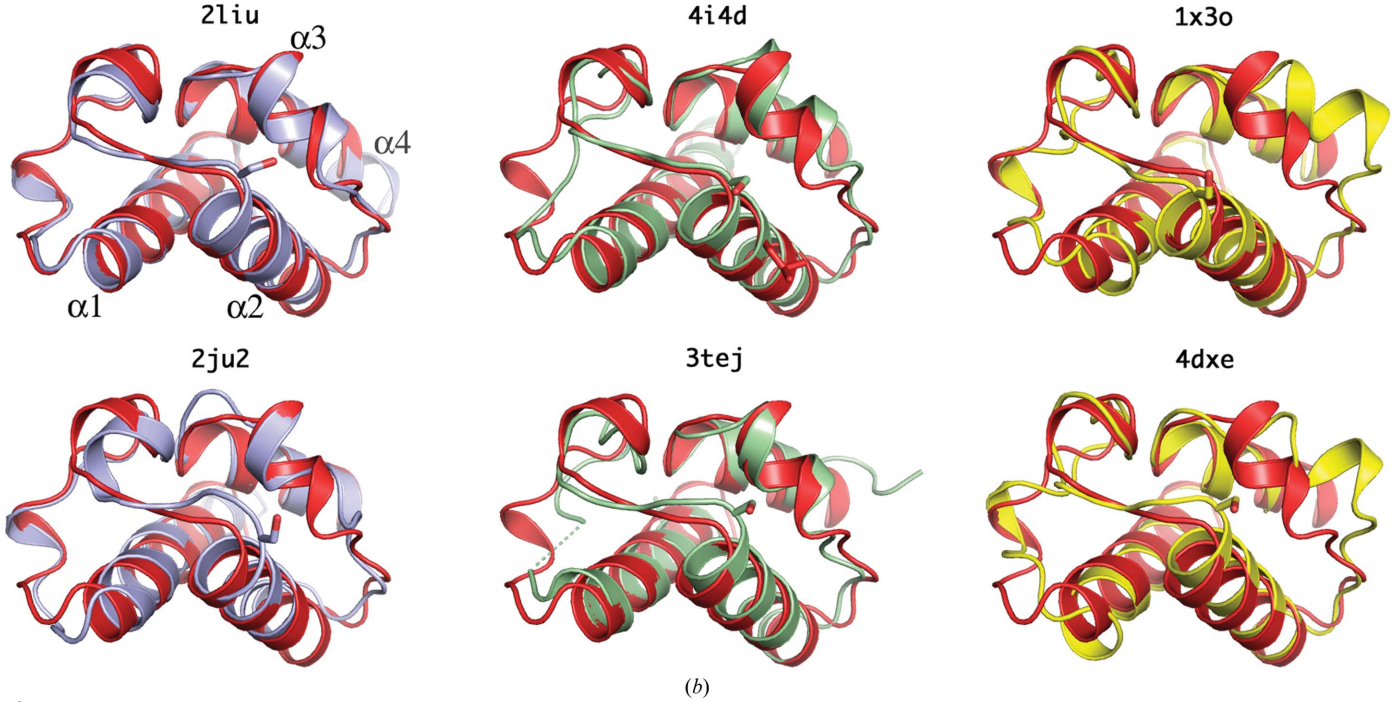

(*b*)

Figure 2
The 14 structures of closest homologs as identified by the *DALI* server were compared with A3404. (*a*) Sequence alignment of the homologous proteins. The first three columns represent the rank in the *DALI* scoring, the type of protein and the PDB code. Proteins in the top half of the alignment are from NPRS or PKS clusters, while proteins in the bottom half are ACPs from fatty-acid synthesis and transport. The pantetheinylation motif is highlighted in yellow; helices $\alpha2$ and $\alpha3$ are shaded in pink. In the alignment, acidic amino acids are red, while basic residues are blue. (*b*) A ribbon diagram of A3404 (red) is superimposed on the top two closest homologs of each of the three carrier protein types. The same orientation is used in all panels and the helix designations are shown in the top left panel. The two PKS acyl carrier proteins 2liu and 2ju2 are shown in light blue. Two NRPS PCP domains, the type II 4i4d and the type I 3tej, are shown in green. Two acyl carrier proteins (1x3o and 4dxe) are shown in yellow. In all structures, the serine residue at the start of helix $\alpha2$ is shown in a stick representation.

differences in the loop between helices $\alpha1$ and $\alpha2$, and, most strikingly, the orientation of the $\alpha3$ helix. This potentially reflects the predominantly acidic nature of the loop immediately before this helix.

Fig. 2(*b*) presents the structures of carrier protein domains from the perspective of the partner protein. The right half of the molecules represents helices $\alpha2$ and $\alpha3$ and the loop that joins them. What is striking from the sequence alignment is the number of negatively charged residues in this region of the ACPs of FAS systems. Of the seven sequences shown, there are an average of more than seven aspartic or glutamic acid residues within this 25-residue stretch. In contrast, the carrier proteins from PKS or NRPS systems show only an average of less than two anionic residues. The A3404 protein has six glutamic acid residues. It seems, however, that this does not imply that A3404 is an ACP from fatty acid metabolism. Rather, this appears to be a function of the type II nature of this protein. BlmI, the recently characterized type II PCP (Lohman *et al.*, 2014), has five acidic residues, as do SgcC2 and MdpC2, two additional type II PCPs from hybrid NRPS/PKS systems (Van Lanen *et al.*, 2006, 2007). It is possible, then, that the highly acidic nature of this region of the protein does not reflect the specific function of the protein as an ACP or PCP but is rather a requirement of the type II carrier proteins. These three proteins, along with A3404, contain the cluster of negatively charged residues at the C-terminal end of helix $\alpha2$; however, none of them contains the anionic residues at the N-terminal portion of this helix.

The first glycine of the pantetheine attachment motif is the most highly conserved residue of the PF00550 family, not including the serine that serves as the necessary pantetheine attachment site. The φ and ψ angles of this residue in A3404 are 94.7 and 2.6°, respectively, in chain *A*, and 97.8 and 0.7°, respectively, in chain *B*. These angles place this residue in a region of the Ramachandran plot that is not allowed for all side-chain-bearing residues. These angles are highly conserved in the closest homologous carrier proteins, including BlmI (85.4 and 12.3°), CurA (142.6 and 5.5°) and the DEBS synthase (112.0 and 56°). This glycine residue is positioned at the end of the 3_{10}-helix and allows the chain to adopt a uniform path to the start of the $\alpha2$ helix. In the 12 structures in Table 2 that contain a glycine at this position, the φ angles range from 63 to 142° and the ψ angles range from −6 to 88°. It appears that this is a structurally conserved configuration that is consistent in a wide variety of carrier protein structures either in isolation or interacting with catalytic domains. The two proteins structures that do not contain a glycine here show main-chain torsion angles φ, ψ of −50, −26° (PDB entry 2afd, residue Asp44) and 74, 85° (PDB entry 2koq, residue Asp37). This highly strained position in the *Streptomyces coelicolor* ACP structure lies just outside the allowable region of the Ramachandran plot for a nonglycine residue.

4. Conclusion

Our laboratory is interested in the production of novel natural products, and in particular we have focused our attention on the NRPS enzymes that are responsible for the production of peptide siderophores. Using the enterobactin and pyoverdine systems of *E. coli* and *P. aeruginosa*, respectively, we have determined the structures of several NRPS domains and associated enzymes. To expand these efforts, we have begun to pursue a novel cluster from the human pathogen *A. baumannii*. The A3404 protein is part of an operon derived from the ABBFA_003406–ABBFA_003399 genes of *A. baumannii* strain AB307-0294 (Adams *et al.*, 2008). Recent studies have demonstrated that genetic disruptions of this operon result in reductions in bacterial motility (Clemmer *et al.*, 2011) and biofilm formation (Rumbo-Feal *et al.*, 2013). This report represents our initial structural characterization of a protein within this pathway. Structural, biochemical and biological experiments are under way to isolate and identify the product of this novel pathway.

The current study presents the structure of a novel carrier protein that is encoded within this biosynthetic operon. Here, we have presented the three-dimensional structure of this protein and compared the sequence and structural features with those of related carrier protein domains from both primary (fatty-acid biosynthesis) and secondary (polyketide and nonribosomal peptide) pathways. The proteins of these processes share many structural features, owing to their shared function, namely the delivery of covalently attached substrates to a variety of interacting catalytic domains. The expression of type II carrier proteins as isolated proteins may pose different demands on their sequence and structure. For example, the free-standing proteins need to bind to their partners intermolecularly in the crowded cellular environment and may therefore require a higher affinity for their partners. Additionally, the solubility requirements for a small isolated protein may result in different global properties than for a domain that is integrated into a larger type I system.

From the structure of A3404, we have identified the features that it shares with carrier proteins of other natural product (NRPS and PKS) systems. The low pI of carrier proteins has been noted previously (Crosby & Crump, 2012; Mercer & Burkart, 2007); however, we have identified potential regions that may be required by free-standing carrier proteins from these different systems. Understanding the structural features of carrier proteins and the interfaces that they form with partner catalytic domains is a valuable step toward characterizing the potential interactions between different proteins of the NRPS and PKS pathways. Similarly, the modular nature of NRPS clusters has raised the potential for engineering these pathways to produce novel peptide products. Clearly, an improved understanding of the key elements that allow functional interactions between the carrier and catalytic domains is necessary for these efforts to succeed.

This work was funded in part by NIH Grant GM-068440 and a grant awarded from and administered by the Telemedicine and Advanced Technology Research Center (TATRC) of the US Army Medical Research and Materiel Command (USAMRMC), Award No. W81XWH-11-2-0218.

Diffraction data were collected at the Stanford Synchrotron Radiation Laboratory, a national user facility operated by Stanford University on behalf of the US Department of Energy, Office of Basic Energy Sciences. The SSRL Structural Molecular Biology Program is supported by the Department of Energy, Office of Biological and Environmental Research, and by the National Institutes of Health National Center for Research Resources, Biomedical Technology Program and the National Institute of General Medical Sciences. We also thank Anyango Kamina for assistance with protein production and crystallization.

References

Adams, M. D., Goglin, K., Molyneaux, N., Hujer, K. M., Lavender, H., Jamison, J. J., MacDonald, I. J., Martin, K. M., Russo, T., Campagnari, A. A., Hujer, A. M., Bonomo, R. A. & Gill, S. R. (2008). *J. Bacteriol.* **190**, 8053–8064.

Adams, P. D. *et al.* (2010). *Acta Cryst.* D**66**, 213–221.

Alekseyev, V. Y., Liu, C. W., Cane, D. E., Puglisi, J. D. & Khosla, C. (2007). *Protein Sci.* **16**, 2093–2107.

Beld, J., Sonnenschein, E. C., Vickery, C. R., Noel, J. P. & Burkart, M. D. (2014). *Nat. Prod. Rep.* **31**, 61–108.

Busche, A., Gottstein, D., Hein, C., Ripin, N., Pader, I., Tufar, P., Eisman, E. B., Gu, L., Walsh, C. T., Sherman, D. H., Löhr, F., Güntert, P. & Dötsch, V. (2011). *ACS Chem. Biol.* **7**, 378–386.

Carter, C. W. Jr & Carter, C. W. (1979). *J. Biol. Chem.* **254**, 12219–12223.

Clemmer, K. M., Bonomo, R. A. & Rather, P. N. (2011). *Microbiology*, **157**, 2534–2544.

Crosby, J. & Crump, M. P. (2012). *Nat. Prod. Rep.* **29**, 1111–1137.

Deng, J., Davies, D. R., Wisedchaisri, G., Wu, M., Hol, W. G. J. & Mehlin, C. (2004). *Acta Cryst.* D**60**, 203–204.

Du, L. & Shen, B. (1999). *Chem. Biol.* **6**, 507–517.

Fischbach, M. A. & Walsh, C. T. (2006). *Chem. Rev.* **106**, 3468–3496.

Gallagher, J. R. & Prigge, S. T. (2010). *Proteins*, **78**, 575–588.

Gross, H. & Loper, J. E. (2009). *Nat. Prod. Rep.* **26**, 1408–1446.

Guy, J. E., Whittle, E., Moche, M., Lengqvist, J., Lindqvist, Y. & Shanklin, J. (2011). *Proc. Natl Acad. Sci. USA*, **108**, 16594–16599.

Haines, A. S. *et al.* (2013). *Nature Chem. Biol.* **9**, 685–692.

Holm, L. & Rosenström, P. (2010). *Nucleic Acids Res.* **38**, W545–W549.

Howard, A., O'Donoghue, M., Feeney, A. & Sleator, R. D. (2012). *Virulence*, **3**, 243–250.

Jancarik, J. & Kim, S.-H. (1991). *J. Appl. Cryst.* **24**, 409–411.

Johnson, M. A., Peti, W., Herrmann, T., Wilson, I. A. & Wüthrich, K. (2006). *Protein Sci.* **15**, 1030–1041.

Kapust, R. B., Tözsér, J., Fox, J. D., Anderson, D. E., Cherry, S., Copeland, T. D. & Waugh, D. S. (2001). *Protein Eng.* **14**, 993–1000.

Keatinge-Clay, A. T. (2012). *Nat. Prod. Rep.* **29**, 1050–1073.

Kissinger, C. R., Gehlhaar, D. K., Smith, B. A. & Bouzida, D. (2001). *Acta Cryst.* D**57**, 1474–1479.

Koglin, A., Mofid, M. R., Löhr, F., Schäfer, B., Rogov, V. V., Blum, M. M., Mittag, T., Marahiel, M. A., Bernhard, F. & Dötsch, V. (2006). *Science*, **312**, 273–276.

Lai, J. R., Koglin, A. & Walsh, C. T. (2006). *Biochemistry*, **45**, 14869–14879.

Li, J. W.-H. & Vederas, J. C. (2009). *Science*, **325**, 161–165.

Liu, Y., Zheng, T. & Bruner, S. D. (2011). *Chem. Biol.* **18**, 1482–1488.

Lohman, J. R., Ma, M., Cuff, M. E., Bigelow, L., Bearden, J., Babnigg, G., Joachimiak, A., Phillips, G. N. Jr & Shen, B. (2014). *Proteins*, doi:10.1002/prot.24485.

Meinwald, J. (2011). *J. Nat. Prod.* **74**, 305–309.

Mercer, A. C. & Burkart, M. D. (2007). *Nat. Prod. Rep.* **24**, 750–773.

Mitchell, C. A., Shi, C., Aldrich, C. C. & Gulick, A. M. (2012). *Biochemistry*, **51**, 3252–3263.

Otwinowski, Z. & Minor, W. (1997). *Methods Enzymol.* **276**, 307–326.

Pettersen, E. F., Goddard, T. D., Huang, C. C., Couch, G. S., Greenblatt, D. M., Meng, E. C. & Ferrin, T. E. (2004). *J. Comput. Chem.* **25**, 1605–1612.

Płoskoń, E., Arthur, C. J., Kanari, A. L., Wattana-amorn, P., Williams, C., Crosby, J., Simpson, T. J., Willis, C. L. & Crump, M. P. (2010). *Chem. Biol.* **17**, 776–785.

Ramelot, T. A. *et al.* (2012). *Biochemistry*, **51**, 7239–7249.

Rumbo-Feal, S., Gómez, M. J., Gayoso, C., Álvarez-Fraga, L., Cabral, M. P., Aransay, A. M., Rodríguez-Ezpeleta, N., Fullaondo, A., Valle, J., Tomás, M., Bou, G. & Poza, M. (2013). *PLoS One*, **8**, e72968.

Samel, S. A., Schoenafinger, G., Knappe, T. A., Marahiel, M. A. & Essen, L. O. (2007). *Structure*, **15**, 781–792.

Smith, M. G., Gianoulis, T. A., Pukatzki, S., Mekalanos, J. J., Ornston, L. N., Gerstein, M. & Snyder, M. (2007). *Genes Dev.* **21**, 601–614.

Strieker, M., Tanović, A. & Marahiel, M. A. (2010). *Curr. Opin. Struct. Biol.* **20**, 234–240.

Vallenet, D. *et al.* (2008). *PLoS One*, **3**, e1805.

Van Lanen, S. G., Lin, S., Dorrestein, P. C., Kelleher, N. L. & Shen, B. (2006). *J. Biol. Chem.* **281**, 29633–29640.

Van Lanen, S. G., Oh, T.-J., Liu, W., Wendt-Pienkowski, E. & Shen, B. (2007). *J. Am. Chem. Soc.* **129**, 13082–13094.

Winn, M. D. *et al.* (2011). *Acta Cryst.* D**67**, 235–242.

Zornetzer, G. A., Fox, B. G. & Markley, J. L. (2006). *Biochemistry*, **45**, 5217–5227.